PERGAMON

International Journal of Multiphase Flow 28 (2002) 199–223

International Journal of Multiphase Flow

www.elsevier.com/locate/ijmulflow

Computational study of fluctuating motions and cluster structures in gas–particle flows

Eivind Helland *, Rene Occelli, Lounes Tadrist

IUSTI-CNRS (UMR 6595), University of Provence, Technopole de Chateau Gombert, 5, rue Enrico Fermi, 13453 Marseille Cedex 13, France

Received 30 September 2000; received in revised form 6 June 2001

Abstract

Simulations with four-way coupling are performed for two-dimensional gas–solid flows in a fluidized bed. The motion of particles is treated by a Lagrangian approach and particles are assumed to interact through binary, instantaneous, non-frontal, inelastic collisions with friction. The model for the interstitial gas phase is based on the Navier–Stokes equations for two-phase flow. The numerical approach has been validated with experimental investigations of the fluctuating motion in a shallow fluidized bed and of cluster characteristics in a fast-fluidized bed. Further on, the influence of the interparticle collision characteristics on the cluster structures and the fluctuating gas–solid motion in diluted flows has been investigated.

Keywords: Gas–particle flows; Clusters; Fluctuating motion; Numerical simulation

1. Introduction

Heterogeneous structures of particles in fluid–particle flows have been observed by a number of authors both in liquid–solid and gas–solid systems (Wilhelm and Kwauk, 1948; Kaye and Boardman, 1962; Jayaweera et al., 1964; Matsen, 1982; Yerushalmi and Avidan, 1985; Fortes et al., 1987; Cattieuw, 1992; Horio and Kuroki, 1994; Horio, 1995; Azario, 1995; Van Den Moortel, 1998).

In fluidized systems most of the particles form aggregates, or clusters, which are regions of high particle concentration compared to the mean solid concentration in the riser. This group of particles moves as an ensemble with only minor relative motions (Fig. 1). Agglomerates are particles held together by inherent interparticle forces and clusters are groups of particles held

* Corresponding author. Tel.: +33-4-42429051.
E-mail address: hellane@bp.com (E. Helland).

0301-9322/02/$ - see front matter
PII: S0301-9322(01)00041-6

Fig. 1. Cluster structures in a circulated fluidized bed (Van Den Moortel, 1998).

together as a result of hydrodynamic effects (Horio and Clift, 1992). In multi-particle systems, the drag accounts for the combination of different effects. Kaye and Boardman (1962) showed that interaction between particles cannot be ignored at solid concentrations higher than 0.05%. Based on their experimental results of cluster formation in dilute suspensions, they divided the behavior of particle suspensions into four distinct regions:

- free-settling at very low particle concentrations,
- a region of viscous interaction in which the group of particles fall faster than individual particles (solid concentrations varying from 0.1% up to 3%) due to cluster formation,
- an unstable region where clusters form and the return flow is irregular and localized; the two phenomena are counteracting (up to a solid concentration of about 10%),
- a well-defined region at higher concentrations where return flow predominates and hindered settling is the dominant feature of the suspension.

Similarities between the cluster formation in liquid–solid and gas–solid systems were evoked by Chen et al. (1991). These authors conducted a similarity analysis to study the hydrodynamics of a multi-particle suspended system. They recognized that the drag is the only source which promotes relative motion between particles and considered that any two systems would have the same tendency of clustering if the drags in these systems are hydrodynamically similar.

The study of clusters has received a great deal of attention during the last decade resulting in a large number of numerical works on fluidized beds (Gidaspow, 1994; Tanaka et al., 1996; Hoomans et al., 1998; Ito et al., 1998; Ouyang and Li, 1999). In a previous work, the axial solid velocity of isolated particles was found to be significantly lower than for particles moving in clusters during their period of formation (Helland et al., 2000; Helland, 2000). Fluctuations in the solid velocity are related to the fluctuations in the solid concentration as accelerations of the solid phase correspond to the bypass of clusters or denser solid phases. An experimental investigation showed that the local solid velocities of up-flowing clusters increased linearly with their size (Van

Den Moortel, 1998). Thus the amplitude of the velocity fluctuations seems to depend on the cluster size.

Shida and Kawai (1989) showed that dissipation of kinetic energy through particle-to-particle collision causes clusters to form even without fluid effects. Tanaka et al. (1996) and Hoomans et al. (1998) stated that the influence of the collision parameters play an important role in the formation of clusters in diluted vertical risers. McNamara and Young (1994) studied numerically the clustering behavior as a function of inelastic collisions. They distinguished three different regimes depending on the restitution coefficient: kinetic regime, cluster regime and the inelastic collapse regime where the particles are stuck together with no relative motion.

In this paper, the numerical approach has been validated by comparison of experimental works of the oscillating motion in a shallow fluidized bed (Clark et al., 2000) and of the cluster characteristics in a fast-fluidized bed (Sharma et al., 2000). Once validated, the influence of the collision characteristics on the fluctuating behavior and the cluster structures in diluted gas–particle flows have been investigated.

2. Physical model

2.1. Equations for the fluid phase

The Eulerian/Lagrangian approach computes the Navier–Stokes equation for the gas phase and the motion of individual particles by the Newtonian equations of motion. For the gas phase, we write the equations of conservation of mass and momentum:

$$\frac{\partial(\varepsilon\rho_{\mathrm{G}})}{\partial t}+\nabla\cdot(\varepsilon\rho_{\mathrm{G}}\vec{u}_{\mathrm{G}})=0, \tag{1}$$

$$\frac{\partial(\varepsilon\rho_{\mathrm{G}}\vec{u}_{\mathrm{G}})}{\partial t}+\nabla\cdot(\varepsilon\rho_{\mathrm{G}}\vec{u}_{\mathrm{G}}\vec{u}_{\mathrm{G}})=-\varepsilon\nabla\cdot(p\bar{\bar{I}})+\nabla\cdot\varepsilon\bar{\bar{\tau}}_{\mathrm{G}}+\varepsilon\rho_{\mathrm{G}}\vec{g}-\sum_{i=1}^{Np(V)}\vec{f}_{\mathrm{drag},i}, \tag{2}$$

where $\vec{g}$ is the gravity acceleration, p is the gas pressure, $\vec{u}_{\mathrm{G}}$ is the gas velocity, ε is the void fraction or porosity, ρ_{G} is the gas density, $\bar{\bar{\tau}}_{\mathrm{G}}$ is the gas stress tensor and $\vec{f}_{\mathrm{drag}}$ is the volumetric drag force. The coupling term $\sum_{i=1}^{Np(V)}\vec{f}_{\mathrm{drag},i}$ between the gas and the particle phase is estimated as the sum of the drag on each particle within the corresponding fluid control volume (Crowe et al., 1977). The meaning of turbulence in gas–particle laden flows has been subject to many discussions (Peirano, 1998; He and Simonin, 1994; Elghobashi, 1994; Lavieville, 1997). In order to simplify the problem, we suppose that the dissipation term of the gas phase due to the turbulence in this configuration is negligible as inertia of the particles damps out the high frequency turbulent scales in the gas phase.

2.2. Equations for the solid phase

In discrete particle models for each individual particle an equation of motion is solved during the free flight phase:

$$m_i\frac{\mathrm{d}\vec{v}_i}{\mathrm{d}t}=m_i\vec{g}+\vec{F}_{\mathrm{drag}}-V_{\mathrm{p}}\nabla p, \tag{3}$$

where m_i, v_i and V_p represent, respectively, the mass, the velocity and the volume of the ith particle and the right-hand side the sum of the forces acting on the ith particle; the first term is due to gravity, the second due to drag between the gas and solid phase and the third the pressure gradient force. The unsteady forces have been neglected due to the high solid to gas density ratio. The slip/rotation or Magnus lift force and the slip/shear or Saffman lift force have also been neglected due to the lack of knowledge in many-particle systems. The drag force is quantified through the equation:

$$\vec{F}_{\text{drag}} = \frac{C_d}{8}\pi d_p^2 \rho_G \varepsilon^2 |\vec{u}_G - \vec{v}_i|(\vec{u}_G - \vec{v}_i) = \frac{C_{d,i}}{8}\pi d_p^2 \rho_G |\vec{u}_G - \vec{v}_i|(\vec{u}_G - \vec{v}_i)\varepsilon^2 f(\varepsilon)^m, \tag{4}$$

where C_d is the drag coefficient and d_p is the particle diameter. Schiller and Naumann (1935) give the drag coefficient $C_{d,i}$ on a single sphere:

$$C_{d,i} = \begin{cases} 24(1 + 0.15Re_p^{0.687})/Re_p, & Re_p < 1000, \\ 0.44, & Re_p \geqslant 1000, \end{cases} \tag{5}$$

where Re_p is the particle Reynolds number

$$\frac{\varepsilon \rho_G |\vec{u}_G - \vec{v}_i| d_p}{\mu_G}.$$

Most of the data for particle drag in many-particle systems have been inferred from sedimentation and uniform fluidization studies. Two opposing clustering effects have been observed depending on the concentration of particles. In regions with few particles distributed non-uniformly, the descent of a given particle can create a velocity field throughout the fluid which tends to decrease the drag of all particles near it due to bypassing of return flow (Gunn and Malik, 1967; Kaye and Boardman, 1962). On the other hand, if the particles are more or less uniformly distributed through the fluid, the restriction of the flow spaces between the particles in denser zones results in steeper velocity gradients of the gas phase, thus greater shearing stresses and an increase in resistance of the gas flow. $f(\varepsilon)$ is a porosity function correcting the terminal velocity or the slip velocity of a particle due to the presence of other particles (hindered settling effect) as they affect the flow pattern in a uniform suspension (Richardson and Zaki, 1954):

$$f(\varepsilon) = \varepsilon^{-n} \tag{6}$$

with

$$n = \frac{\log(Re_{mf}/Re_t)}{\log \varepsilon_{mf}}, \tag{7}$$

where Re_{mf} is the Reynolds number at minimum fluidization (drag equals the weight of the particles in the settled bed at maximum concentration, $\varepsilon = \varepsilon_{mf}$, i.e., minimum fluidization condition), and Re_t, the Reynolds number at terminal velocity $U_{t,0}$ (drag equals the weight of an isolated particle $\varepsilon = 1$).

If the restricted flow within the cluster were uniformly distributed in a manner similar to the original flow away from it, n would be unity. However, the interstitial gas flow will be unevenly distributed within the cluster due to different physical conditions from particle to particle, thus the value of n results from an averaging of these effects. Thus its value depends on the nature of the

interstitial gas flow (laminar/turbulent) and this was discussed thoroughly in the paper of Maude and Whitmore (1958). Experimental workers have reported values of n between 2 and 4 for spheres in turbulent flow; n close to 5 for equi-sized, equi-density spheres in creeping flow; and n between 7 and 10 for rough particles in creeping flow. The value of m (Eq. (4)) varies between 1 and 2 depending on the particle Reynolds number as the porosity function corrects the terminal velocity or the slip velocity in a fluid–solid suspension ($U_t = U_{t,0}\varepsilon^n$ and $U_{\mathrm{mf}} = U_{t,0}\varepsilon_{\mathrm{mf}}^n$ (minimum fluidization velocity)). The parameter m is equal to 1 for laminar interstitial flow ($Re_{\mathrm{p}} < 1$), 2 for turbulent interstitial flow ($Re_{\mathrm{p}} > 1000$) and an intermediate value in the transition regime ($1 < Re_{\mathrm{p}} < 1000$). Based on these results Maude and Whitmore (1958) and Wen and Yu (1966) proposed a general relation for the sedimentation and fluidization for mono-dispersed spheres in laminar ($m = 1$ and $n = 4.7$), intermediate and turbulent interstitial regimes ($m = 2$ and $n = 2.35$). Their drag function is used in this study and can be expressed:

$$C_{\mathrm{d}} = C_{\mathrm{d},i} f(\varepsilon)^m = C_{\mathrm{d},i}\varepsilon^{-4.7}. \tag{8}$$

Different drag corrections are used in literature and having in common an increasing drag coefficient with particle concentration.

Eq. (3) can be rewritten as:

$$\frac{\mathrm{d}\vec{v}_i}{\mathrm{d}t} = \vec{g} + \frac{1}{\tau_{i\mathrm{G}}}(\vec{u}_{\mathrm{G}} - \vec{v}_i) - \frac{1}{\rho_{\mathrm{p}}}\nabla p \tag{9}$$

with

$$\tau_{i\mathrm{G}} = \frac{\rho_{\mathrm{p}} d_{\mathrm{p}}^2}{18\mu_{\mathrm{G}}(1 + 0.15 Re_{\mathrm{p}}^{0.687})}\varepsilon^{3,7} \tag{10}$$

valid in the laminar and the transition regime ($Re_{\mathrm{p}} < 1000$).

The particle relaxation time $\tau_{i\mathrm{G}}$ decreases exponentially as the local porosity decreases indicating that the drag force influences the fluid–particle flow radically stronger as solid concentration increases.

2.3. Collision model

In particulate multiphase flows, collision occurs between the particles or between the particle and the wall. A collision without permanent deformation or heat generation is called an elastic collision. Otherwise, the collision is inelastic and energy loss occurs mainly in the form of permanent deformation suck as particle breakage and frictional heat loss (Fan and Zhu, 1998). The collision model proposed by Wang and Mason (1992) is used to compute the dynamics of instantaneous inelastic non-frontal collisions with friction based on three constant coefficients. The first coefficient e characterizes the incomplete restitution of the normal component of the relative velocity at the point of contact. The second μ arises in collisions involving sliding and has been described by Coulomb friction. The third β arises in collisions that return a fraction of the energy stored in the elastic deformation of both surfaces to the component of the contact velocity tangent to the spheres.

We consider two particles of diameter d_1 and d_2 and with masses m_1 and m_2. The positions of the sphere centers are described by the vectors $\vec{r}_1$ and $\vec{r}_2$. The unit normal $\vec{n}$ at the contact point is defined by:

$$\vec{n} = \frac{\vec{r}_1 - \vec{r}_2}{|\vec{r}_1 - \vec{r}_2|}. \tag{11}$$

The relative velocity $\vec{v}_c$ between the two particles at the contact point is given by:

$$\vec{v}_c = \vec{v}_1 - \vec{v}_2 - \left(\frac{d_1}{2}\vec{\omega}_1 + \frac{d_2}{2}\vec{\omega}_2\right) \times \vec{n}, \tag{12}$$

where $\vec{v}_i$ and $\vec{\omega}_i$ are, respectively, the translation and angular velocities before impact. The impact angle γ is defined as the angle between the normal $\vec{n}$ and the relative velocity $\vec{v}_c$ such that $\gamma \in [\frac{\pi}{2}, \pi]$.

Fig. 2(a) shows the situation of two particles before collision with $\vec{\omega}_1 = \vec{\omega}_2 = \vec{0}$. We consider the conservation of kinetic momentum of translation during the collision where $\vec{v}_i'$ represent the velocities after collision:

$$\Delta\vec{P} = m_1(\vec{v}_1' - \vec{v}_1) = -m_2(\vec{v}_2' - \vec{v}_2). \tag{13}$$

The normal component of $\Delta\vec{P}$ does not affect the angular velocities. However, the tangential component $\Delta\vec{P}^{(t)}$ provokes a variation of the rotational momentum. Fig. 2(b) represents the situation after impact. We can calculate the velocities after impact if we know the variation of momentum $\Delta\vec{P}$:

$$\vec{v}_1' = \vec{v}_1 + \frac{\Delta\vec{P}}{m_1}, \tag{14}$$

$$\vec{v}_2' = \vec{v}_2 - \frac{\Delta\vec{P}}{m_2}, \tag{15}$$

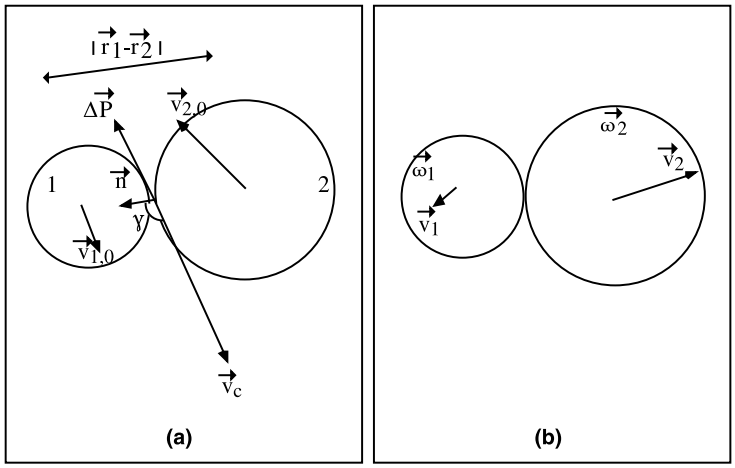

Fig. 2. Two particles before (a) and after (b) impact.

$$\vec{\omega}_1' = \vec{\omega}_1 - \frac{d_1}{2I_1}\vec{n} \times \Delta\vec{P}, \tag{16}$$

$$\vec{\omega}_2' = \vec{\omega}_2 - \frac{d_2}{2I_2}\vec{n} \times \Delta\vec{P}. \tag{17}$$

The Coulomb friction law neglects the fact that an object can pivot on another object. Instead of developing a complex model, it is common to introduce a tangential restitution coefficient β. Foerster et al. (1994) showed that the variation of momentum $\Delta\vec{P}$ during impact could be written:

$$\Delta\vec{P} = -m_{12}(1+e)\vec{v}_c^{(n)} - \frac{2}{7}m_{12}(1+\beta)\vec{v}_c^{(t)}, \tag{18}$$

where $m_{12} = (m_1^{-1} + m_2^{-1})^{-1}$ is the reduced mass. It is defined that $e = 1$ for the normal impact of perfect elastic spheres (no loss of kinetic energy), while $e = 0$ for the normal impact of perfect plastic spheres. The coefficient of restitution in an impact depends not only on the material properties of the colliding objects but also on their relative impact velocity (Gorham and Kharaz, 2000). In this study, we suppose that the coefficient of restitution is independent of the relative impact velocity.

For great values of the impact angle $\gamma \geqslant \gamma_0$ (micro-slip region), the tangential restitution coefficient for glass spheres was found $\beta_0 \in [0.35, 0.50]$. For small impact angles $\gamma \leqslant \gamma_0$, we define $\beta_1 = -1 - (7/2)\mu(1+e)\cot\gamma$. This is the sliding region where the interaction between the particles during impact can be described by the Coulomb friction coefficient μ and the restitution coefficient e. Foerster et al. (1994) showed experimentally that the model describes well the behavior of the impact between glass spheres over a wide range of incident angles.

3. Numerical solution technique

Eqs. (1) and (2) are solved by a finite volume method. The SIMPLE scheme is used as iterative solution procedure (Patankar, 1980). A staggered grid is used with velocity components stored at the control volume surfaces and the scalar variables at the center. The integration of the conservation equations is performed using the Quick scheme in space and an implicit scheme in time.

The velocity components of the particles and their positions are calculated directly after Eq. (9). We use a semi-implicit method in order to avoid iterations on the velocities:

$$\vec{v}_i|_{t+\Delta t_p} = \left(\frac{\vec{v}_i|_t}{\Delta t_p} + \vec{g} + \frac{\vec{u}_G|_{t+\Delta t_f}}{\tau_{ig}(\vec{u}_G|_{t+\Delta t_f}, \vec{v}_i|_t, \varepsilon|_t)} - \frac{1}{\rho_p}\vec{\nabla}p|_{t+\Delta t_f} \Big/ \frac{1+\Delta t_p}{\tau_{iG}(\vec{u}_g|_{t+\Delta t_f}, \vec{v}_i|_t, \varepsilon|_t)} \right) \Delta t_p. \tag{19}$$

Each particle's corresponding gas velocity and porosity in Eq. (19) are estimated by linear interpolation depending on its position within the fluid control volume (FCV). Two time scales are distinguished in the model, which means that two different time steps are used. A *fluid time step* Δt_f is used to solve the equations for the fluid phase. This time step is chosen to be smaller than the particle relaxation time τ_{iG} at maximum packing concentration. Within the fluid time step several *particle time steps* Δt_p is used for the hard-sphere particle simulations. A minimum particle time step Δt_p^c is defined such that any particle having the actual maximum gas velocity only can pass a length equal to 20% of the particle diameter:

$$\Delta t_{\mathrm{p}}^{\mathrm{c}} = \frac{0.2 d_{\mathrm{p}}}{\max |\vec{u}_{\mathrm{g}}|}. \tag{20}$$

This calculated time step $\Delta t_{\mathrm{p}}^{\mathrm{c}}$ is used if it is less than the particle time step Δt_{p} defined by the user.

The fluid control volume is taken large enough to have a representative elementary volume in order to estimate the porosity accurately, but little enough to have small changes in flow properties. Once the particles have been moved by interaction with the gas and gravity (Eq. (9)), we start the search of overlapping between particles within the riser in order to treat the collision dynamics. In order to save CPU time several *particle control volumes* (PCV) within the FCV are used. We have developed an algorithm for detection of particle overlapping within each PCV. Every particle within a PCV (*i* particles) and its adjacent PCVs (*j–i* particles) are included in a list of *j* particles (Fig. 3). The list includes only the adjacent PCVs in one direction (Fig. 4), however, in the next particle time step, we change the direction of sweeping through the numerical domain.

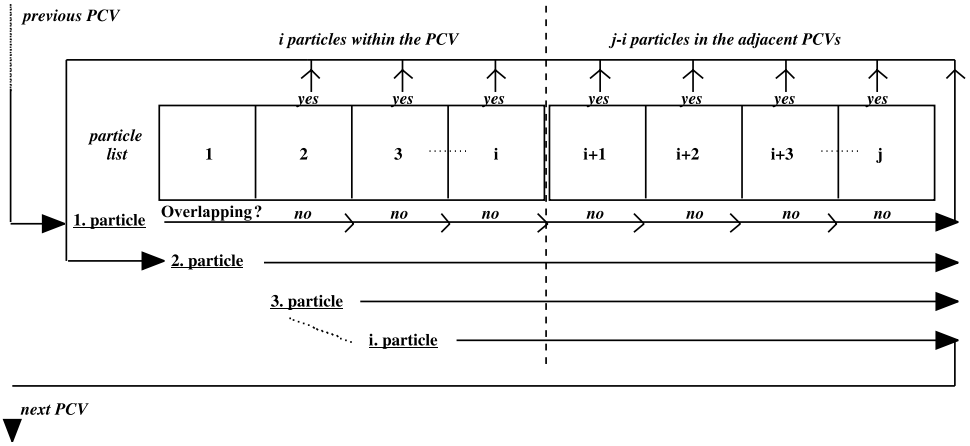

Fig. 3. Algorithm for detection of particle overlapping.

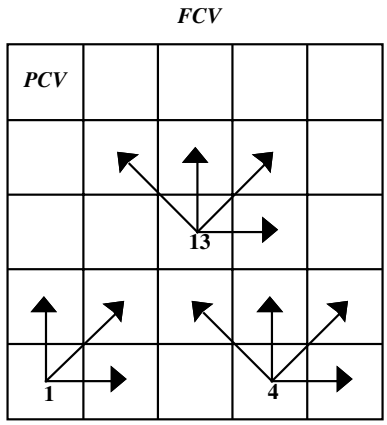

Fig. 4. Adjacent PCVs included in the collision list.

We try to include as many PCVs within an FCV as possible in order to make the collision list as small as possible. The minimum size of the PCV is only limited by the particle size.

For the first particle in the collision list, we search for overlapping with the other $j-1$ particles. When a first overlapping has been detected, we treat the collision dynamics for the two particles involved. For the first particle the search for overlapping is terminated. Then, we repeat the searching procedure for the next $(i-1)$ particles in the list. For these particles, we only search for overlapping with the subsequent particles. When all of the i particles within the respective PCV have undergone the procedure, we repeat the same treatment for the next PCV until every collision list for all the PCVs in the calculation domain has been treated.

By this method, there is a risk of missing some collisions in the denser particle regions. Nevertheless, this method seems to be efficient as no or an insignificant fraction of particle overlapping is observed even in zones of high particle concentrations.

The value of the contact angle, γ^* at the moment of detection does not necessarily correspond to the actual value γ at the moment of contact (Fig. 5). If numerical overlapping occurs, the particle positions are rearranged with the aid of the relative velocities, and the new positions are assigned to the actual moment of contact, then the collision dynamics is calculated inducing a change of the translation and rotation velocities and the position of the two particles.

The two-dimensional porosity in a computational cell is the ratio of the surface occupied by the gas to the surface of the fluid control volume ΔS. If S_i is the surface of particle i inside a computational cell, then the porosity in this cell is:

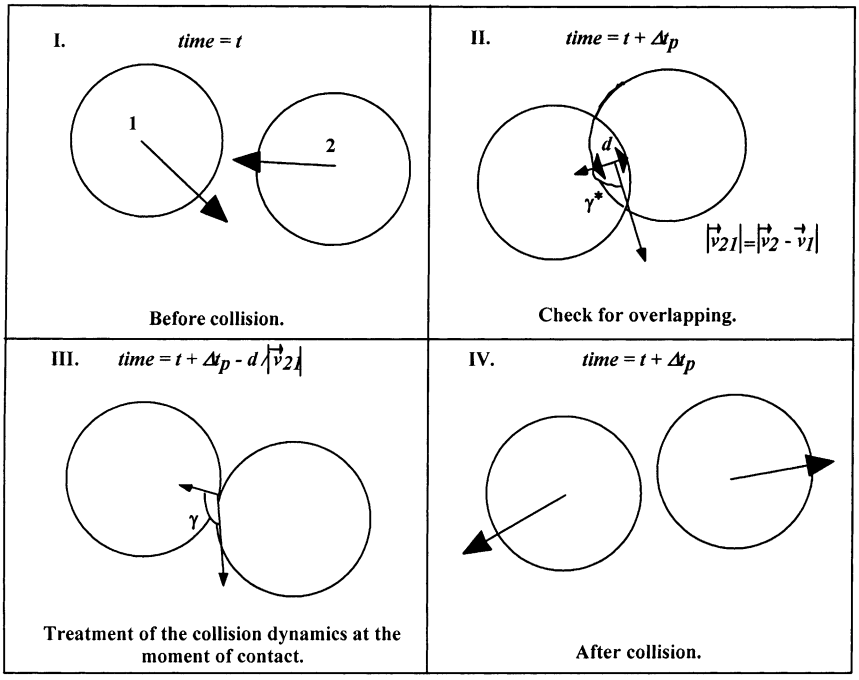

Fig. 5. Strategy of collision dynamics calculation.

$$\varepsilon_{2D} = 1 - \sum_{i=1}^{N_c} S_i/\Delta S \tag{21}$$

The porosity calculated in this way is based on a two-dimensional analysis, which is inconsistent with the applied empiricism in the calculation of the drag force exerted on a particle. Therefore, we utilize a pseudo-three-dimensional concept in which we assume the depth of the bed equal to the particle diameter. Thus the porosity estimation is corrected in order to use the drag force for a sphere.

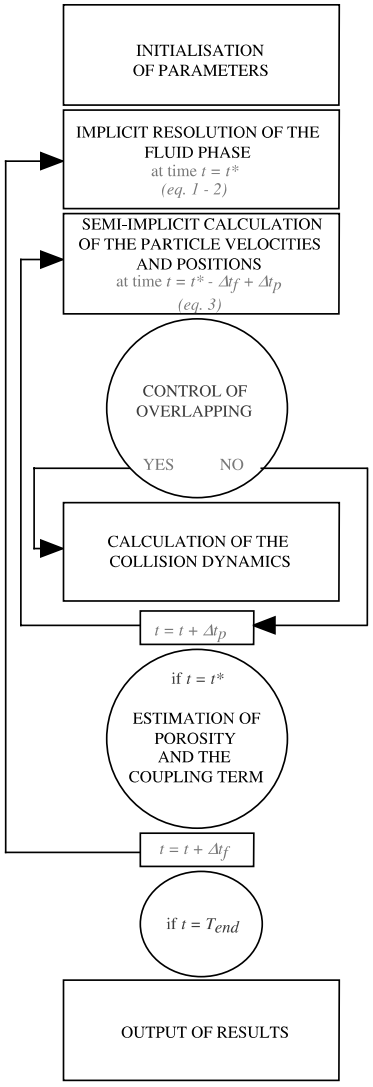

Fig. 6. Numerical procedure of the gas–particle flow resolution.

$$\varepsilon_{3D} = 1 - \frac{2}{3}(1 - \varepsilon_{2D}). \tag{22}$$

The numerical procedure can be schematized as shown in Fig. 6. The gas motion is calculated at instant $t + \Delta t_f$ with the drag force estimated at instant t. Then the particle positions are calculated at the next *particle time step* $t + \Delta t_p$, followed by the treatment of the collision dynamics. After finding the new velocities and positions of all particles at instant $t + \Delta t_f$, the void fraction is estimated and the drag forces on every particle summarized within each fluid control volume.

Clusters are certainly three-dimensional structures in the riser, thus experimental and two-dimensional numerical results may not be quantitatively comparable.

The air inlet is modeled as one-dimensional uniform flow. In the simulations, the outlet is located at the top of the riser where a continuity condition is used for the gas phase. The particles leaving at the top are simultaneously introduced at the bottom of the riser at random positions with zero velocities. A no-slip condition is used for the gas phase at the walls and the particles are allowed for frontal collisions at the wall controlled by the wall coefficient of restitution e_w.

4. Results and discussion

4.1. Validation of the numerical approach

4.1.1. Oscillations in a shallow fluidized bed

In this section, we report a study of comparison between numerical and experimental results of the dynamic behavior in a shallow fluidized bed. The different parameters used in this study are presented in Table 1. Clark et al. (2000) measured the pressure frequency of the large-scale layer oscillations as a function of bed depth (between 3 and 7 particles deep).

Table 1
Parameter settings

Superficial gas velocity	0.15 m/s
Particle diameter, d_p	150 μm
Density (particle, gas), ρ_p, ρ_G	8800 kg/m^3, 1.2 kg/m^3
Gas viscosity, μ_G	1.8×10^{-5} kg/m/s
Restitution coefficient, e	0.9
Wall rest. coeff. e_w	0.9
Tangential restitution coefficient, β	0.5
Coulomb friction coefficient, μ	0.1
Riser width, D	0.15 m
Riser height, H	0.15 m
Number of particles	800
Grid number (nx, ny)	FCV: (15, 15)–PCV: (3, 3)
Re_p	25
Minimum τ_{iG}	0.008 s
Fluid time step	$\Delta t_f = 10^{-5}$ s
Particle time step	$\Delta t_p = 10^{-6}$ s

These large-scale fluctuations occur due to formation of bubbles during fluidization and their collapsing at the surface. For superficial gas velocities below the terminal velocity, an isolated particle is at rest at the bottom of the riser. When increasing the number of particles in its neighborhood, we observe a motion of particles within the riser. This is due to both an increase in gas velocity as the efficient surface decreases and, more important, an increase in drag due to greater shearing stresses as the flow spaces between the particles are restricted. If we have locally perturbations of the porosity within the bed, the drag is increasing where the particle phase is denser. This gives rise to particle zones of different accelerations and we experience a formation of void zones or "bubbles" in regions of higher accelerations (Fig. 7). Once developed the gas chooses the easiest way up, thus an exceed of gas flow in the void zone and the bubble increases in size. When the bubble rises, there is a raining of particles from its roof due to smaller particle group effect on the drag for the particles situated at the bubble interface (self-sharpening effect due to an important porosity gradient). When loosing the grip of the dense particle group, the interfacial particles behave as single particles falling down as gravity dominates their drag and raining is observed. When the bubbles erupt at the bed surface, the surrounding particles are ejected upwards in the riser. Thus the particles are more or less isolated with fewer influences of the many-particle effect on the drag force. The particles drop back into the bottom zone as gravity

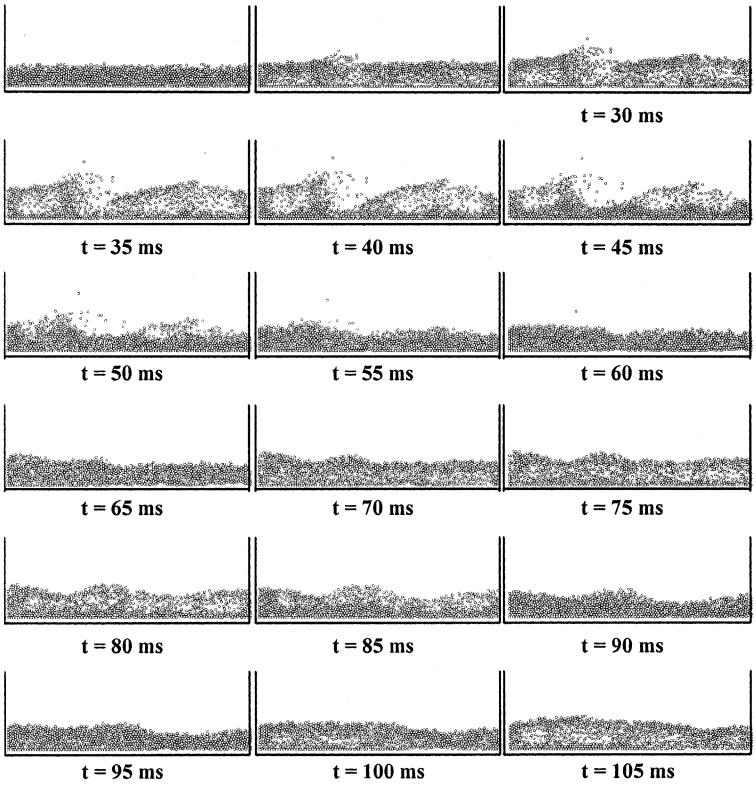

Fig. 7. Time sequence of the oscillating behavior ($t = 20$–105 ms).

dominates the drag for superficial gas velocities below the terminal velocity. This gives rise to a fluctuating gas–particle motion in the fluidized bed. Earlier works have been concentrated on the origin of this fluctuating motion and the prediction of the fluctuation frequency (Hiby, 1967; Baskakov et al., 1986; Roy et al., 1990). Previous theories to predict oscillations in a fluidized bed give a measure of the natural frequency of oscillations. Baskakov et al. (1986) treated the fluid bed like liquid oscillating in a U-tube with a frequency of oscillation equal to $\frac{1}{\pi}\sqrt{g/h_{\mathrm{mf}}}$, where h_{mf} is the bed height at minimal fluidization condition. This is the characteristic time scale of a particle dropping behind the bubble a distance close to the bed height.

Fig. 8 represents the time evolution of the pressure drop in the bed. The pressure oscillates around an average value equal to 60 Pa with a period between 30 and 40 ms. The theoretical pressure drop based on the bed weight is equal to 54 Pa. When comparing Figs. 7 and 8, we observe that maximum pressure drop corresponds to the moment of bubble formation ($t = 20$, 60 and 90 ms). The bed expands and the fluid "chooses" a preferential route with smaller resistance and the pressure drop decreases to value below the total bed weight until the bubble eruption at the bed surface. Then, a new cycle starts with a maximum pressure drop.

The numerical results show a period of oscillation close to 35 ms (29 Hz). This value is comparable with the theory proposed by Baskakov et al. (1986) (32 Hz) and the measured frequency from the experimental results of Clark et al. (2000) (32.5 Hz) when the bed height is equal to 1 mm. The numerical approach describes the evolution of the pressure fluctuations measured by others in a shallow bed. This may be explained by the fact that the three-dimensional effects are not so important in this experimental configuration.

4.1.2. Cluster characteristics in a fast-fluidized bed

Sharma et al. (2000) investigated the effect of particle size and superficial gas velocity on the duration time, occurrence frequency, time-fraction of existence and solid concentration in clusters by capacitance-probe measurements of instantaneous local solid concentration in a 15 cm fast-fluidized bed. Their cluster definition was based on the following three guidelines given by Soong et al. (1993):

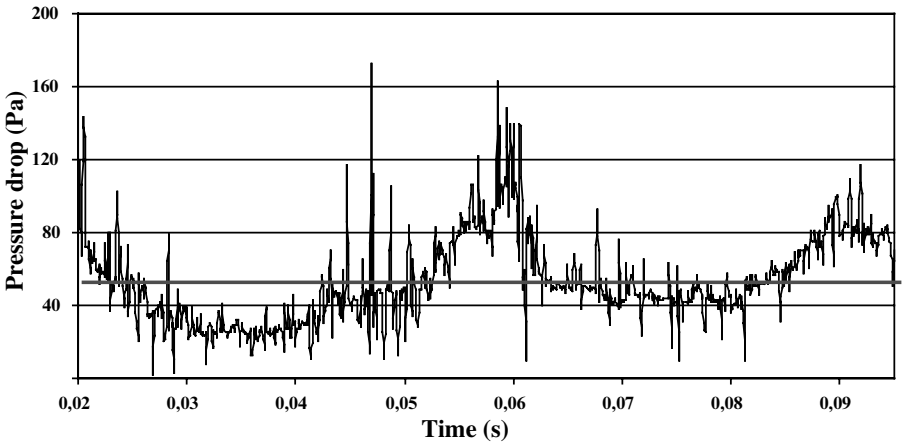

Fig. 8. Time evolution of the pressure drop in the fluidized bed.

- The solid concentration in a cluster must be significantly above the time-average solid concentration at the given local position, for the given operating condition.
- This perturbation in solid concentration due to clusters must be greater than the random background fluctuations of the solid fraction.
- This concentration perturbation should be sensed for sampling volume with characteristic length scale greater than one to two orders of particle diameter.

Sharma et al. (2000) proposed the following criteria for the period of cluster life:

- The cluster is detected once the instantaneous solid concentration is greater than two times its standard deviation (2σ).
- The starting time of a cluster is the last time its density exceeds the mean density before satisfying the 2σ criterion.
- The ending time of a cluster would be the first time the density falls below the mean solid concentration, after falling below the 2σ limit.

The numerical and experimental results of three superficial gas velocities and a particle diameter of 120 μm have been compared. All studies were made at a constant solid flux close to 75 kg/m^2/s. In order to save CPU time, we reduced the riser height and diameter. The numerical results represent the flow behavior in the upper part of the riser where the axial solid concentration profile is constant. Sharma et al. (2000) showed that the axial pressure profiles were linear after a 1.9 m distance from the riser feed point. Their experiments were carried out at a height of 4.5 m above the riser feed point. The parameter settings are summarized in Table 2.

To illustrate the application of the criterion of Sharma et al. (2000), Fig. 10 shows an expansion of the transient signal for the numerical run plotted in Fig. 9, from 1.00 to 1.14 s. Fig. 10 represents the auto-scaled solid concentration ε_s^*, which is defined as:

Table 2
Parameter settings

Particle diameter, d_p	120 μm
Density (solids, gas) ρ_p, ρ_G	2400 kg/m^3, 1.2 kg/m^3
Gas viscosity, μ_G	1.8×10^{-5} kg/m/s
Superficial gas velocity	4.0, 4.9, 6.6 m/s
Restitution coefficient, e	0.97
Wall rest. coeff. e_w	0.85
Tangential restitution coefficient, β	0.5
Coulomb friction coefficient, μ	0.1
Riser width	0.075 m
Riser height	0.5 m
Total solids concentration	1%
Grid number (nx, ny)	FCV: (30, 100)–PCV: (15, 30)
Re_p	10
Minimum τ_{iG}	0.002 s
Fluid time step	$\Delta t_f = 5 \times 10^{-4}$ s
Particle time step	$\Delta t_p = 5^*10^{-5}$ s

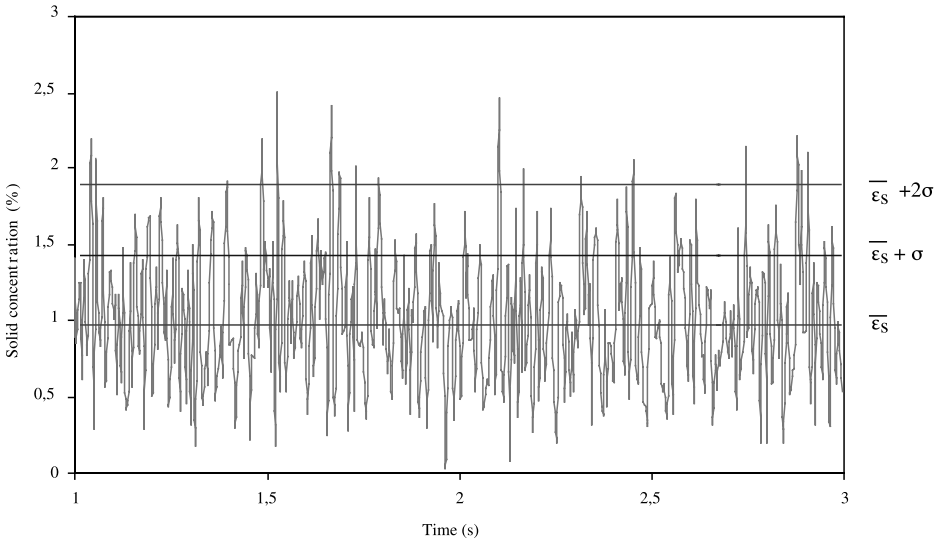

Fig. 9. Transient variations in solid concentration in the center of the riser ($(x, y) = (3.75\text{ cm}, 37.5\text{ cm})$, $U_g = 4.9$ m/s).

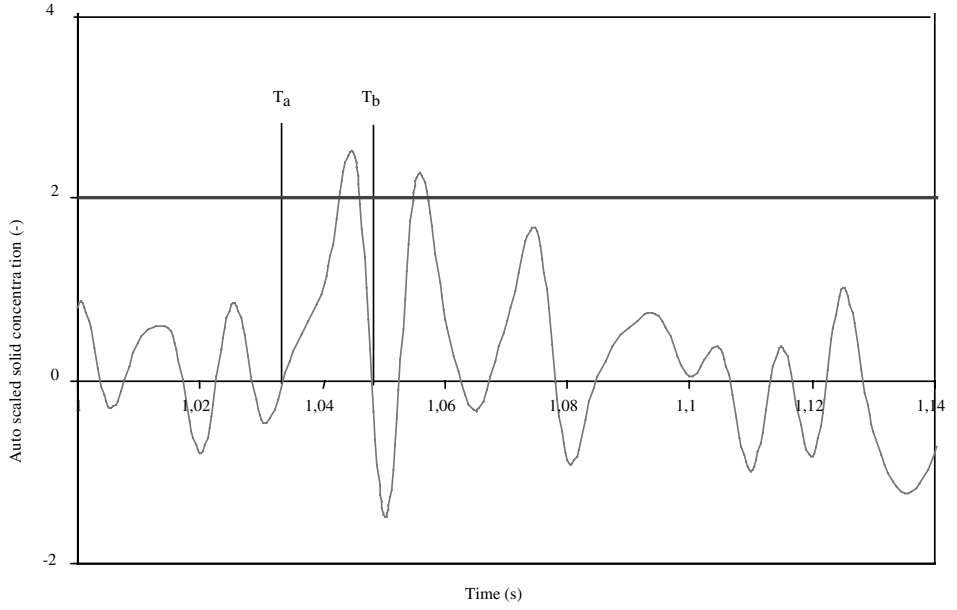

Fig. 10. Short-time scale trace of the auto-scaled solid concentration in the center of the riser ($(x, y) = (3.75\text{ cm}, 37.5\text{ cm})$, $U_g = 4.9$ m/s).

$$\varepsilon_s^* = \frac{\varepsilon_s - \overline{\varepsilon_s}}{\sigma}. \tag{23}$$

On this scale, the time-averaged solid concentration is the zero ordinate and the vertical scale represents multiples of the standard deviation. Fig. 10 shows the transient signal relative to the

time-mean and to the 2σ threshold. This small sample illustrates two clusters during the 0.14 s interval. In particular, one cluster is observed between times T_a and T_b.

In the following, we have compared the parametric effect of superficial gas velocity on different characteristics of clusters in the center of the riser: number-averaged cluster duration time, frequency of cluster occurrence and time fraction of cluster existence. Referring to Fig. 10, the time length $\tau_i = T_b - T_a$ is the duration for which the ith cluster is observed. The number-averaged duration time is then:

$$\tau_c' = \frac{\sum_{i=1}^{n} \tau_i}{n}, \tag{24}$$

where n is the total number of clusters detected in an observation period τ ($\tau = 5$ s simulation time). The frequency of cluster occurrence (N) is the frequency at which clusters are observed at the sampling volume, calculated as the average number of clusters observed per second, over the total observation time, τ. The cluster existence time fraction (F) is the fraction of total time when clusters exists at the sampling volume. This quantity is calculated as the ratio of total cluster duration time to total observation time.

A parametric plot of (N) versus superficial gas velocity presented in Fig. 11 shows that the frequency of cluster occurrence is between 6 and 9 clusters/s for the experimental results while it varies between 7 and 12 clusters/s for the numerical results.

In Fig. 12, we have presented the values of the cluster duration time in the center of the riser. The experimental results show an increase in duration time with the superficial gas velocity (from 10 to 16 ms) while the numerical results indicate values between 12 and 15 ms with no obvious gas velocity trend. Nevertheless, the results show up to have the same order of magnitude.

Sharma et al. (2000) raised an interesting question in their paper: what fraction of the time do clusters exist at a given position, and what is the effect of the superficial gas velocity and particle

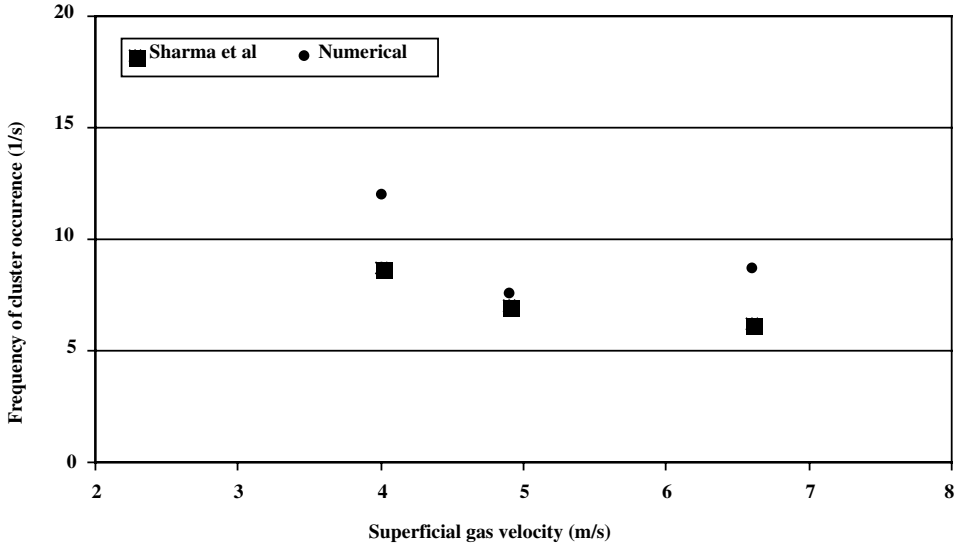

Fig. 11. Frequency of cluster occurrence in the center of the riser: $(x, y) = (3.75 \text{ cm}, 37.5 \text{ cm})$.

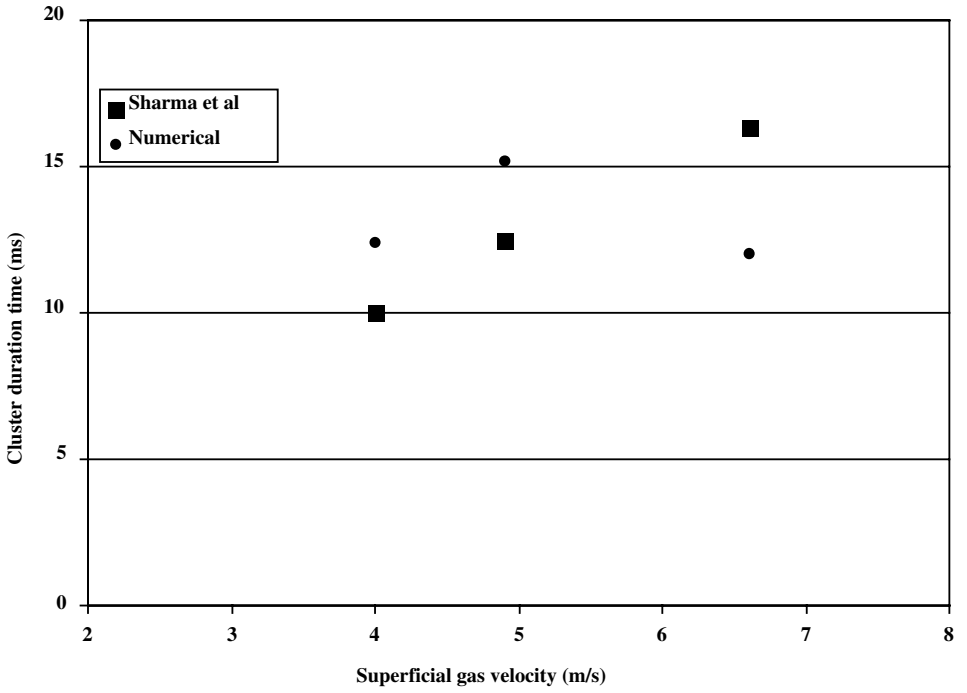

Fig. 12. Number averaged cluster duration time in the center of the riser: $(x, y) = (3.75\text{ cm}, 37.5\text{ cm})$.

diameter on this fraction? In their paper, they presented only cross-section averaged time fractions and not local time fractions. They found that neither gas velocity nor particle diameter affected the time fraction of cluster presence. In six different cases, all values were found to lie between 0.16 and 0.18. As they claimed, we should expect that a 65% variation of gas velocity would alter the population density of clusters and thus affect the time fraction. Their experimental results show that the time duration of a cluster in the wall region is of an order of magnitude greater that those in the core zone of the riser. The clusters are likely to be trapped closed to the walls, thus the cross-averaged value of cluster characteristics are strongly affected by wall effects.

In Fig. 13, we show the local time fraction of cluster existence in the center of the riser versus superficial gas velocity. These numerical results show a decrease in the local time fraction of about 50% when increasing the gas velocity (from 0.15 to 0.10). Ouyang and Li (1999) reported a similar tendency in a numerical study. Clusters became smaller when increasing the superficial gas velocity, until they nearly vanished at a sufficient high gas velocity.

The numerical approach describes fairly well different cluster characteristics observed experimentally by Sharma et al. (2000) in a fast-fluidized bed. This comparative study shows that numerical approaches can be complementary to experimental investigations.

4.2. Influence of the collision characteristics on the cluster structures in a diluted gas–particle flow

In this section, we carry out a study of the collision parameters and their influence on the fluctuating bed behavior and the cluster structures. The parameter settings are summarized in

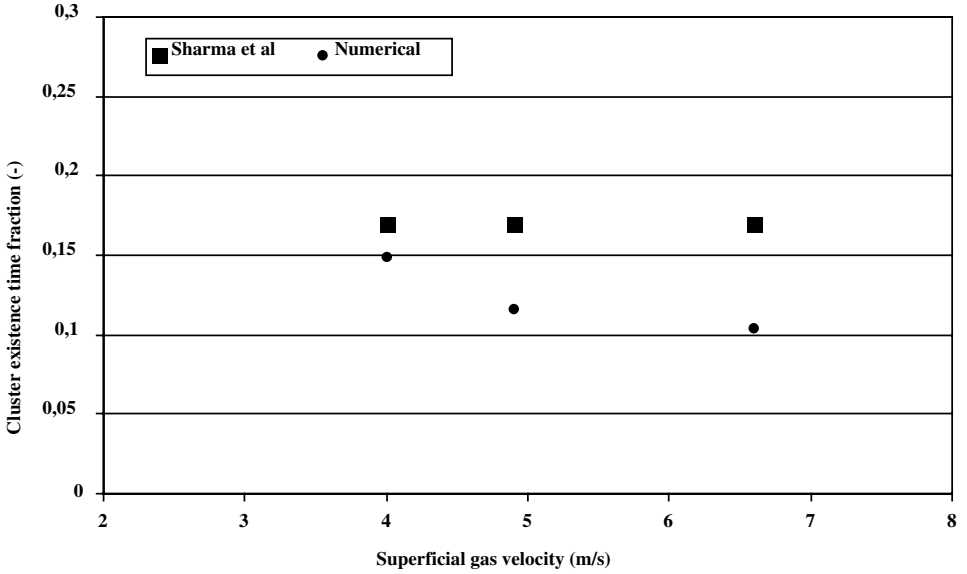

Fig. 13. Cluster existence time fraction time in the center of the riser: $(x, y) = (3.75\text{ cm}, 37.5\text{ cm})$.

Table 3
Parameter settings

Particle diameter, d_p	120 μm
Density (solids, gas) ρ_p, ρ_G	2400 kg/m^3, 1.2 kg/m^3
Gas viscosity, μ_G	1.8×10^{-5} kg/m/s
Superficial gas velocity	2.0 m/s
Restitution coefficient, e	0.3–1.0
Wall rest. coeff. e_w	0.85
Tangential restitution coefficient, β	0.5
Coulomb friction coefficient, μ	0.1–0.7
Riser width	0.05 m
Riser height	1 m
Total solids concentration	1.5%
Grid number (nx, ny)	FCV: (20, 100)–PCV: (17, 22)
Re_p	10
Minimum τ_{iG}	0.002 s
Fluid time step	$\Delta t_f = 10^{-3}$ s
Particle time step	$\Delta t_p = 2 \times 10^{-5}$ s

Table 3. Fig. 14 shows a time series of the gas–particle flow in the lower part of the riser. We observe cluster structures similar to those observed experimentally (Fig. 1). The clusters exhibit horseshoe shapes heading upwards or downwards in the riser. The wall regions behave as collectors of down falling clusters.

Fig. 15 represents a snapshot of the riser at different resolutions. The form of the clusters in the core zone corresponds to the mean gas velocity profile. Once the particles taking part of the

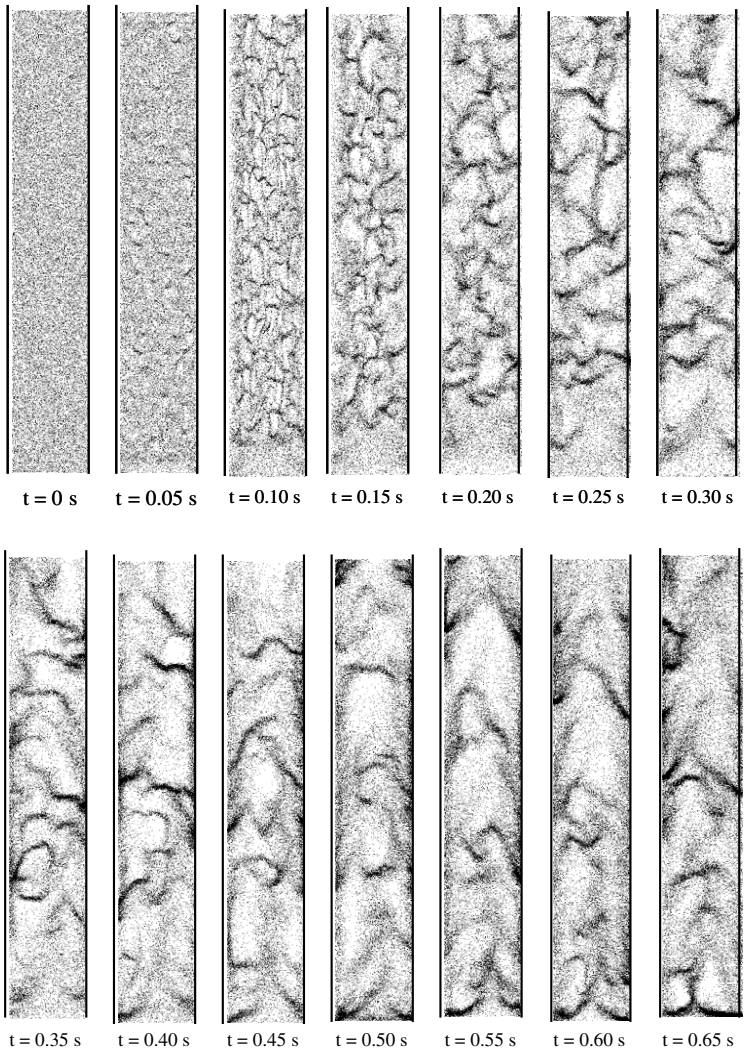

Fig. 14. Time series of the gas–particle flow in the riser. y: (0–30 cm).

clusters are stuck in the wall region, they drop back in the bottom zone collecting particles on their way down. In this way, the wall clusters seem to be denser than the core zone clusters.

Fig. 16 shows the structure of clusters for different values of the restitution coefficient. The inelastic collisions have a significant effect on the density of the clusters as dissipation of kinetic energy decreases the dispersion of particles and the relative motion between particles. When increasing the inelasticity of collisions, the clusters have a higher concentration of particles, they decrease in size and are easier to distinguish from the average gas–particle flow structure. Fig. 17 represents the local porosity of the cluster in the core zone as a function of the restitution coefficient. When decreasing the restitution coefficient, the local porosity within the cluster decreases towards the value of maximum packing (inelastic collapse). If such conditions are reached, the

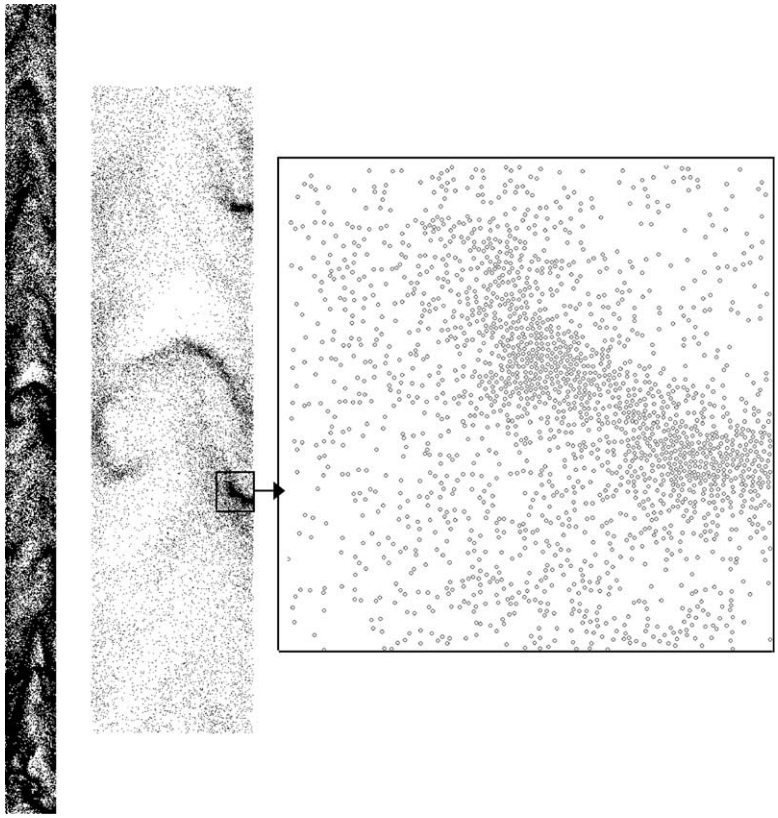

Fig. 15. Cluster structures in the vertical riser: (left) y: (0–80 cm); (middle) y: (30–50 cm); (right): 1.25×1.25 cm^2.

particles within the cluster would be in contact over a longer period and interparticle forces (Van der Waals, liquid bridge forces) should be considered for completeness of the study.

For the denser clusters, the local pressure drop increases, and the gas phase tends to round the obstacle. Therefore, preferential routes are created in the gas–particle flow, giving rise to strong hydrodynamic fluctuations due the coupling between the phases.

Fig. 18 shows the influence of the restitution coefficient on the standard deviation of the axial particle velocity for different transversal positions in the riser. The wall region exhibits strong fluctuations due to the appearance of dense clusters falling down along the wall, and it seems difficult to study the influence of the collision parameters. However, in the core zone, there is a tendency of stronger amplitudes of fluctuations when decreasing the restitution coefficient.

Fig. 19 shows the influence of the restitution coefficient on the mean value of the standard deviation in the core zone of both the axial and transversal particle velocities. The amplitudes of the axial components are about three times higher than the transversal, indicating an anisotropic behavior of the gas–particle properties in the riser. Azario (1995) has observed such behavior experimentally in a circulating fluidized bed.

The inelastic collisions show a strong influence on the fluidized bed behavior. The "small scale fluctuations" due to inter-particle collisions decrease when increasing the inelasticity of the

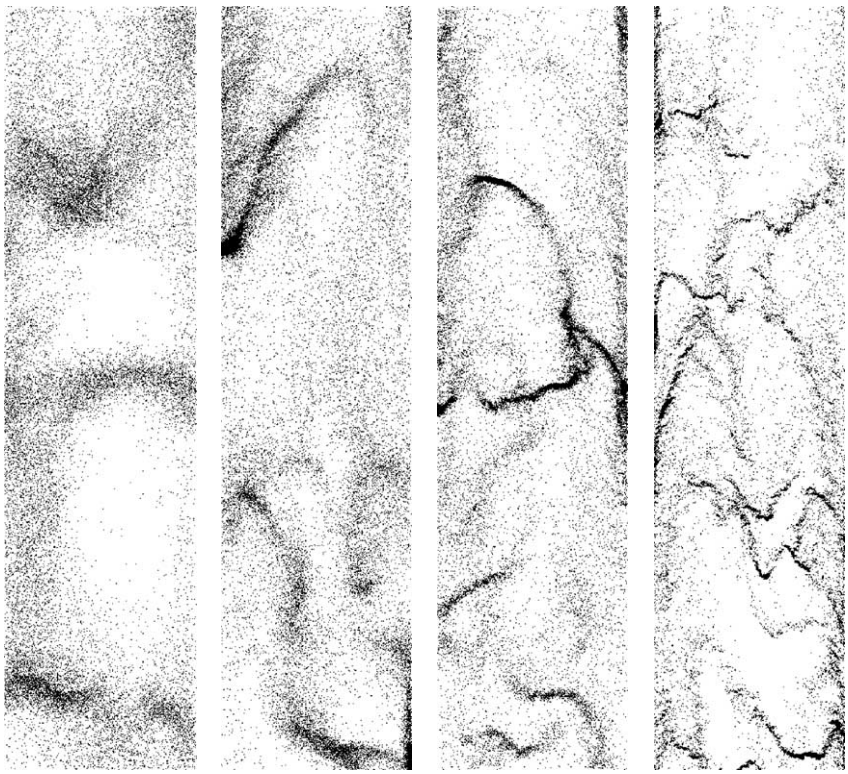

Fig. 16. Cluster structures as a function of the restitution coefficient. y: (30–50 cm). From left to right: $e = 1$, $e = 0.97$, $e = 0.8$ and $e = 0.3$.

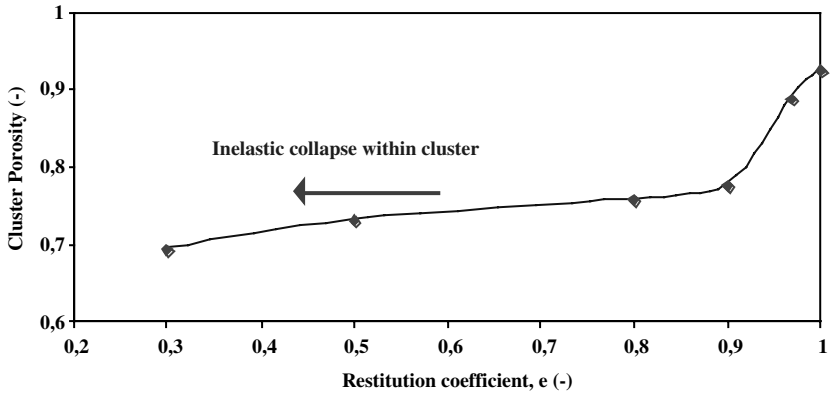

Fig. 17. Local porosity within the cluster as a function of the restitution coefficient.

particles. This results in denser clusters leading to greater "large scale fluctuations" due to stronger variations in local drag.

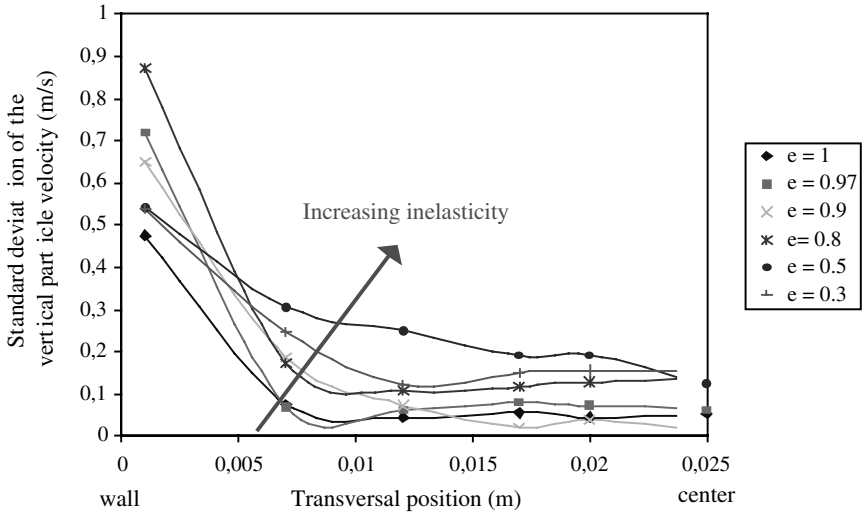

Fig. 18. Influence of the restitution coefficient on the standard deviation of the axial particle velocity as a function of the transversal position.

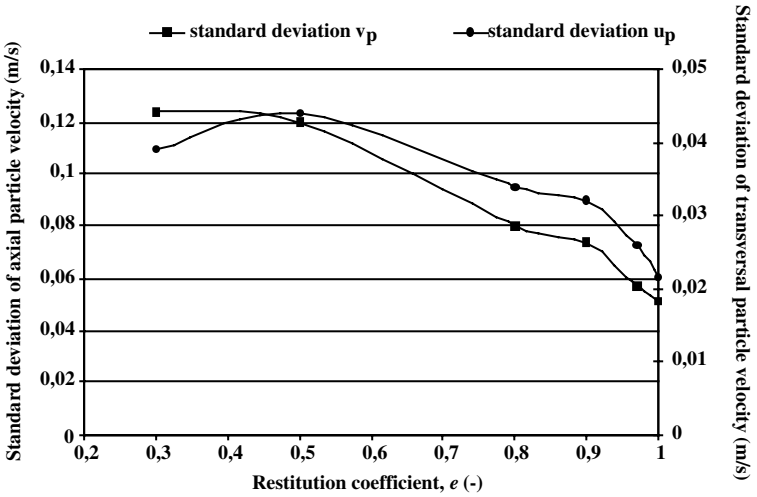

Fig. 19. Standard deviation of the axial and transversal particle velocities as a function of the restitution coefficient in the core zone of the riser.

When increasing the friction coefficient μ, there is an increase in transversal momentum transferred to rotational momentum due to collisions between particles. The results presented in Fig. 20 show a negligible influence of this parameter. This can be interpreted by the fact that transfer of momentum between particles during collisions in our configuration is dominated by the coupling between the gas and particle phases due to drag.

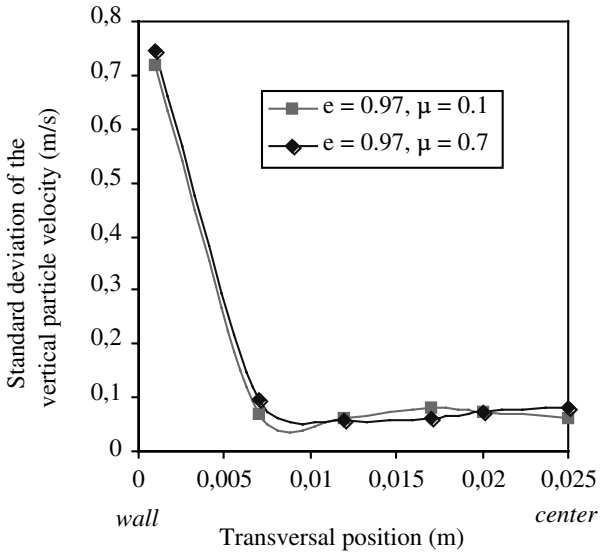

Fig. 20. Influence of the friction coefficient on the standard deviation of the axial particle velocity as a function of the transversal position.

5. Conclusions

We have investigated numerically the gas–particle flow in a vertical two-dimensional configuration. The numerical approach has been validated against instantaneous measurements of the pressure in a shallow fluidized bed by comparing the dominant frequency of oscillations and against instantaneous measurements of the solid concentration in a fast-fluidized bed by comparing cluster duration time, frequency of occurrence and time fraction of cluster existence. The results show a reasonable agreement between the experimental and the numerical approaches.

The following study of clusters shows that the gas–particle properties have a strong anisotropic fluctuating behavior. This instability is linked to both hydrodynamical phenomena and the inelastic interparticle collisions. We observe denser clusters when decreasing the restitution coefficient due to a smaller dispersion of particles during inelastic collisions. This decreases the local porosity within the clusters, which increases the amplitudes of fluctuations caused by a stronger coupling between the phases due to the non-linear influence of local porosity on the drag.

Acknowledgements

The authors show their gratitude to *The French Agency for Environment and Energy Management* (ADEME) for financial assistance.

References

Azario, E., 1995. Analyse locale des caracteristiques hydrodynamiques d'un lit fluidise circulant. Thesis. University of Provence, IUSTI, France.

Baskakov, A.P., Tuponogov, V.G., Filippovsky, N.F., 1986. A study of pressure fluctuations in a bubbling fluidized bed. Powder Technol. 46, 113–117.

Cattieuw, P., 1992. Etude experimentale des ecoulements gaz–particules dans un lit circulant. Thesis. University of Provence, IUSTI, France.

Chen, Y.-M., Jang, C.-S., Cai, P., Fan, L.-S., 1991. On the formation and disintegration of particle clusters in a liquid–solid transport bed. Chem. Eng. Sci. 46 (9), 2253–2268.

Clark, D.K., Tsimring, L.S., Aranson, I.S., (2000) Oscillations and defect turbulence in a shallow fluidized bed, submitted to PRLhttp://www.arvix.org/abs/nlin/0005010.

Crowe, C.T., Sharma, M.P., Stock, D.E., 1977. The Particle-Source-In-Cell (PSICELL) model for gas-droplet flows. J. Fluids Eng. 99, 325–332.

Elghobashi, S., 1994. On predicting particle-laden turbulent flows. Appl. Sci. Res. 52, 309–329.

Fan, L-S., Zhu, C., 1998. Principles of gas–solid flows. In: Collision Mechanics of Solids. Cambridge University Press, Cambridge (Chapter 2).

Foerster, S., Louge, M., Chang, H., Allia, K., 1994. Measurements of the collision properties of small spheres. Phys. Fluids 6, 1108–1115.

Fortes, A.F., Joseph, D.D., Lundgren, T.S., 1987. Nonlinear mechanics of fluidization of beds of spherical particles. J. Fluids Mech. 177, 467–483.

Gidaspow, D., 1994. Multiphase Flow and Fluidization. Academic Press, New York.

Gorham, D.A., Kharaz, A.H., 2000. The measurement of particle rebound characteristics. Powder Technol. 122, 193–202.

Gunn, D.J., Malik, A.A., 1967. The structure of fluidized beds in particulate fluidization. In: Proceedings of International Symposium on Fluidization, Einhoven, pp. 52–65.

He, J., Simonin, O., 1994. Modelisation numerique des ecoulements turbulents gaz–solides en conduite verticale. Report EDF DER LNH HE-44/94/021A.

Helland, E., Occelli, R., Tadrist, L., 2000. Numerical study of cluster formation in gas–particle flow in a circulating fluidized bed. Powder Technol. 110, 210–221.

Helland, E., 2000. Etude des ecoulements fluide-solide dans les lits fluidises: simulation numerique et analyse des heterogeneites Thesis. University of Provence, IUSTI, France.

Hiby, J.W., 1967. Periodic phenomena connected with gas–solid fluidization. In: Proceedings of International Symposium on Fluidization, Eindhoven, pp. 99–109.

Hoomans, B.P.B., Kuipers, J.A.M., Van Swaaij, W.P.M., 1998. Granular dynamics simulation of cluster formation in dense riser flow. In: 3rd International Conference on Multiphase Flow, Lyon, France, pp. 2.7–9.

Horio, M., Clift, R., 1992. A note on terminology: 'clusters' and 'agglomerates'. Powder Technol. 70, 196.

Horio, M., Kuroki, H., 1994. Three-dimensional flow visualization of dilutely dispersed solids in bubbling and circulating fluidized beds. Chem. Eng. Sci. 49, 2413–2421.

Horio, M., 1995. Cluster and agglomeration formation in fluidized suspensions. In: 2nd International Conference on Multiphase Flow, Kyoto, FB1.1–1.12.

Ito, M., Tsukada, M., Shinamura, J., Horio, M., 1998. Prediction of cluster size and slip velocity in circulating fluidized beds by a DSMC model. Fluidization IX. Durango, USA, pp. 525–532.

Jayaweera, K.O.L.F., Mason, B.J., Slack, G.W., 1964. The behaviour of clusters of spheres falling in a viscous fluid. Part I experiment. J. Fluid Mech. 20, 121–128.

Kaye, B.H., Boardman, R.P., 1962, Cluster formation in dilute suspensions. In: Proceedings of the Symposium on Interaction between Fluids and Particles, British Institute of Chemical Engineers, London, pp. 17–21.

Lavieville, J., 1997. Simulations numeriques et modelisation des interaction entre l'entrainement par la turbulence et les collisions interparticulaires en ecoulements gaz–solide, Thesis, University of Rouen, France.

Matsen, J.M., 1982. Mechanisms of choking and entrainment. Powder Technol. 32, 21–33.

Maude, A.D., Whitmore, R.L., 1958. A generalized theory of sedimentation. Brit. J. Appl. Phys. 9, 477–482.

McNamara, S., Young, W.R., 1994. Inelastic collapse in two dimensions. Phys. Rev. E 50, 28–31.
Ouyang, J., Li, J., 1999. Discrete simulations of heterogeneous structure and dynamic behavior in gas–solid fluidization. Chem. Eng. Sci. 54, 5427–5440.
Patankar, S.V., 1980. Numerical Heat Transfer and Fluid Flow. Hemisphere Publishing Corporation, New York.
Peirano, E., 1998. Modelling and simulations of turbulent gas–solid flows applied to fluidization. Thesis, Chalmers University, Sweden.
Richardson, J.F., Zaki, W.N., 1954. Sedimentation and fluidization: Part 1. Trans. Inst. Chem. Eng. 32, 35–53.
Roy, R., Davidson, J.F., Tuponogov, V.G., 1990. The velocity of sound in fluidized beds. Chem. Eng. Sci. 45, 3233–3245.
Schiller, L., Naumann, A.Z., 1935. A drag coefficient correlation. Ver. Deut. Ing. 77, 318–320.
Sharma, A.K., Tuzla, K., Matsen, J., Chen, J.C., 2000. Parametric effects of particle size and gas velocity on cluster characteristics in fast fluidized beds. Powder Technol. 111, 114–122.
Shida, K., Kawai, T., 1989. Cluster formation by inelastically colliding particles in one-dimensional space. Phys. A 159, 145–160.
Soong, C.H., Tuzla, K., Chen, J.C., 1993. Identification of particle clusters in circulating fluidized beds. In: Avidan, A.A. (Ed.), Circulating Fluidized Bed Technology, vol. 4. Engineering Foundation, New York, pp. 615–620.
Tanaka, T., Yonemura, S., Kiribayashi, K., Tsuji, Y., 1996. Cluster formation and particle-induced instability in gas–solid flows predicted by the DCMC method. JSME Int. J., Ser. B 39, 239–245.
Van Den Moortel, T., 1998. Analyse locale des structures d'ecoulements gaz–particules dans un lit fluidise circulant. Thesis. University of Provence, IUSTI, France.
Wang, Y., Mason, M.T., 1992. Two-dimensional rigid body collisions with friction. J. Appl. Mech. 59, 635–642.
Wen, C.Y., Yu, Y.H., 1966. Mechanics of fluidization. Chem. Eng. Prog. Symp. Ser. 62, 100–111.
Wilhelm, R.H., Kwauk, M., 1948. Fluidization of solid particles. Chem. Eng. Progr. 44, 201.
Yerushalmi, J., Avidan, A.A., 1985. In: Davidson, Clift, Harrison (Eds.), Fluidization. Academic Press, London (Chapter 7).